Synthesis and characterization of the chain borosulfates (NH4)3[B(SO4)3] and Sr[B2(SO4)4]

Philip Netzsch, Henning A. Höppe

Angaben zur Veröffentlichung / Publication details:

Netzsch, Philip, and Henning A. Höppe. 2020. “Synthesis and characterization of the chain borosulfates (NH4)3[B(SO4)3] and Sr[B2(SO4)4].” Zeitschrift für anorganische und allgemeine Chemie 646 (18): 1563–69. https://doi.org/10.1002/zaac.202000105.

Journal of Inorganic and General Chemistry
ZAAC
Zeitschrift für anorganische und allgemeine Chemie

DOI: 10.1002/zaac.202000105

ARTICLE

Synthesis and Characterization of the Chain Borosulfates $(NH_4)_3[B(SO_4)_3]$ and $Sr[B_2(SO_4)_4]$

Philip Netzsch[a] and Henning A. Höppe*[a]

Dedicated to Prof. Dr. Bernd Harbrecht on the Occasion of his 70th Birthday

Abstract. Two new borosulfates were obtained either by an open vessel synthesis from sulfuric acid and $B(OH)_3$, yielding $(NH_4)_3[B(SO_4)_3]$ or from solvothermal synthesis in oleum enriched sulfuric acid and $B(OH)_3$, yielding $Sr[B_2(SO_4)_4]$. $(NH_4)_3[B(SO_4)_3]$ crystallizes homeotypic to $K_3[B(SO_4)_3]$ in space group *Ibca* (Z = 8, a = 728.58(3) pm, b = 1470.84(7) pm, c = 2270.52(11) pm), comprising open branched *vierer* single chains $\{^1_\infty[B(SO_4)_2(SO_4)_{2/2}]^{3-}\}$. $Sr[B_2(SO_4)_4]$ crystallizes as an ordered variant of $Pb[B_2(SO_4)_4]$ in space group *Pnna* (Z = 4, a = 1257.4(4) pm, b = 1242.1(4) pm, c = 731.9(2) pm), consisting of loop branched *vierer* single chains $\{^1_\infty[B(SO_4)_{4/2}]^{2-}\}$. Vibrational spectroscopy confirms both refined structure models. Thermal analysis of the dried powders, showed a decomposition towards the binary and ternary components, whereas a thermal treatment in the presence of the mother liquor promotes a decomposition of $Sr[B_2(SO_4)_4]$ towards $Sr[B_2O(SO_4)_3]$.

Introduction

Various material classes such as alumosilicates, nitridosilicates or borophosphates possess analogue tetrahedral fundamental building units TX_4 (T = B, Al, Si; X = N, O) and are accordingly be classified as silicate-analogous materials. The vast structural diversity of silicates[1] and the extraordinary properties of the aforementioned materials inspires material scientists for new substitution variants. In recent times, especially the field of borosulfates comprising corner sharing borate and sulfate tetrahedra has been expanding tremendously.[2] Due to the most common basic building unit, $B(SO_4)_4$, a further analogy towards silicates becomes obvious. Herein, the borate tetrahedra can be seen as central moiety T and the sulfate tetrahedra as terminal moiety X, giving rise for so-called supertetrahedra. These might condense to polymeric structures by common corners, common edges or even forego the bridging sulfate tetrahedra by forming direct B–O–B bridges, comparable to Si–Si bonds – the latter found in nitridosilicates chemistry in $Sr[Si_6N_8]$.[3] Hence, borosulfates offer the potential of an extraordinary structural diversity.

Starting from the first borosulfate $K_5[B(SO_4)_4]$ in 2012,[4] borosulfates with the most basic monovalent cations, especially alkali metals were investigated. Already the alkali metal borosulfates show a vast structural variety, with zero dimensional anions in $K_5[B(SO_4)_4]$,[4] one dimensional anions in $K_3[B(SO_4)_3]$,[5] two dimensional anions in $Cs_2[B_2O(SO_4)_3]$[6] and even three dimensional anions in $Li[B(SO_4)_2]$.[5] Furthermore, several different structures per cation can be synthesized – in case of potassium four different compounds are already reported by now: $K_5[B(SO_4)_4]$, $K_3[B(SO_4)_3]$, $K[B(SO_4)_2]$ and $K[B(S_2O_7)_2]$.[4,5,7,8] However, for ammonium which chemically behaves very similar to potassium, only $NH_4[B(SO_4)_2]$ and $NH_4[B(S_2O_7)_2]$ are known.[7] Expanding research from alkali metal borosulfates towards the slightly more acidic alkaline earth metal borosulfates yielded α- and β-$Mg_4[B_2O(SO_4)_6]$,[9] $M[B_2(SO_4)_4]$ (M = Mg, Ca)[9,10] and $M[B_2O(SO_4)_3]$ (M = Sr, Ba).[11,12] Herein, especially strontium and barium compounds are of interest, since they are promising candidates as host structure for doping with divalent europium. Moreover, the two lead compounds $Pb[B_2O(SO_4)_3]$, which is structurally related to $Sr[B_2O(SO_4)_3]$, and $Pb[B_2(SO_4)_4]$[13] indicate the presence of further strontium borosulfates. Herein, we expand the borosulfate family with crystal structures of two new representatives, namely $(NH_4)_3[B(SO_4)_3]$ and $Sr[B_2(SO_4)_4]$. We characterized them employing X-ray powder diffraction, vibrational spectroscopy, and thermal analysis.

* Prof. Dr. H. A. Höppe
E-Mail: henning.hoeppe@physik.uni-augsburg.de
[a] Chair of Solid State and Materials Chemistry, Institute of Physics
University of Augsburg
Universitaetsstraße 1
86159 Augsburg, Germany

Supporting information for this article is available on the WWW under **http://dx.doi.org/10.1002/zaac.202000105** or from the author.

Results and Discussion

Crystal Structure

$(NH_4)_3[B(SO_4)_3]$

$(NH_4)_3[B(SO_4)_3]$ crystallizes in space group *Ibca* (no. 73) homeotypic to $K_3[B(SO_4)_3]$[5] in the structure type of $Ba_3[B(PO_4)_3]$.[14] The structure consists of corner sharing bor-

ate and sulfate tetrahedra forming open branched *vierer* single chains parallel along the (100) direction (Figure 1). Each borate tetrahedron is connected to four adjacent sulfate tetrahedra, whereas the sulfate tetrahedra can be distinguished between bridging ones – connected to two borate tetrahedra – and terminal ones – connected to one borate tetrahedron. Hence, the anion can be described by the Niggli formula $^{1}_{\infty}[B(SO_4)_2(SO_4)_{2/2}]^{3-}$}. By eying the corner sharing connection pattern of the supertetrahedra with a B:S ratio of 1:3, unbranched *zweier* single chains result, comparable to the silicate chains in $Ag_2[SiO_3]$.[15]

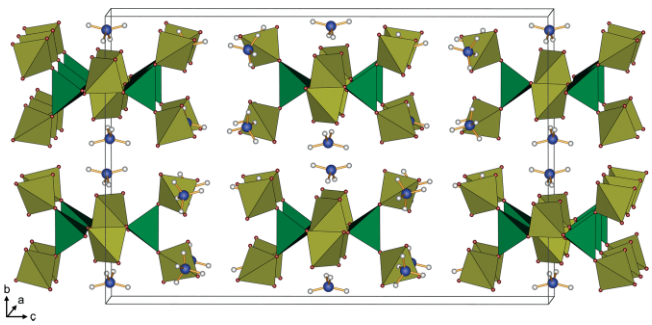

Figure 1. Crystal structure of $(NH_4)_3[B(SO_4)_3]$ viewed along (100); sulfate tetrahedra yellow, borate tetrahedra green, nitrogen atoms blue, and hydrogen atoms white.

Within the borate tetrahedron short B–O^{term} bonds [143.90(13) pm] towards the terminal sulfate tetrahedra occur, whereas the B–O^{br} bonds [149.50(14) pm] towards the bridging sulfate tetrahedra are significantly longer (Table 1). The bridging sulfate tetrahedron exhibits two short S^{br}–O^{term} bonds [143.48(11) pm] towards the terminal oxygen atom and two long S^{br}–O^{br} bonds [152.33(10) pm] towards the bridging oxygen atoms. Similar behavior is found for the terminal sulfate tetrahedron with three short S^{term}–O^{term} bonds [143.91(12) – 145.00(12) pm] and one long S^{term}–O^{br} [157.99(10) pm]. This is in line with the values found for bridging and terminal sulfate tetrahedra in other borosulfates.[5,16] The deviation from the tetrahedral symmetry[17,18] amounts to –0.59 % for the borate tetrahedron and –0.09 % for the terminal sulfate tetrahedron and –0.51 % for the bridging one. Furthermore, the BS_4 supertetrahedron shows a deviation of –2.91 %, which is comparatively small for such huge moieties found in borosulfates.[7]

Table 1. Selected interatomic distances /pm and angles /° in the compounds $(NH_4)_3[B(SO_4)_3]$ and $Sr[B_2(SO_4)_4]$ (esds in parentheses).

	$(NH_4)_3[B(SO_4)_3]$	$Sr[B_2(SO_4)_4]$
M–O		254.0(3)–270.4(3)
$\Sigma r_{ion}(M\text{–O})$[22]		271
S^{br}–O^{br}	152.33(10)	141.7(3)–142.3(3)
S^{br}–O^{term}	143.48(11)	152.6(3)–154.5(3)
S^{term}–O^{br}	157.99(10)	–
S^{term}–O^{term}	143.91(12)–145.00(12)	–
B–O^{br}	149.50(14)	146.5(6)–147.1(6)
B–O^{term}	143.90(13)	–
O–S^{br}–O	97.76(7)–114.98(10)	103.6(2)–117.5(3)
O–S^{term}–O	105.92(6)–114.17(8)	–
O–B–O	106.86(5)–118.4(2)	106.3(4)–114.1(5)

Charge compensation is achieved by NH_4^+ cations embedded by hydrogen bonds towards the terminal oxygen atoms of the sulfate tetrahedra (Figure 2). Both crystallographically independent ammonium cations comprise four hydrogen bonds of moderate strength.[19] The hydrogen-acceptor distances *d*(H-A) range between 185 and 214 pm, the donor-acceptor distances *d*(D-A) range between 276 and 299 pm and the bond angles (DHA) are found between 146 and 175°. The eightfold coordination observed for the potassium cations in $K_3[B(SO_4)_3]$ is retrieved by considering also weak hydrogen bonds[19] with *d*(H–A) in the range from 247 to 284 pm.

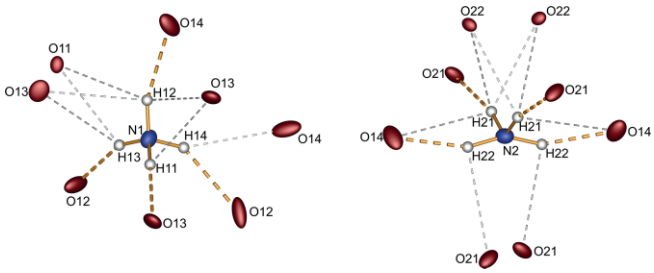

Figure 2. Hydrogen bonds in $(NH_4)_3[B(SO_4)_3]$; moderately strong hydrogen bonds are displayed as thick dashed orange lines, weak hydrogen bonds as thin dashed grey lines.

$Sr[B_2(SO_4)_4]$

$Sr[B_2(SO_4)_4]$ crystallizes in space group *Pnna* (no. 52) as ordered variant of $Pb[B_2(SO_4)_4]$.[13] The structure comprises one dimensional chains of alternating corner sharing borate and sulfate tetrahedra running parallel to the (001) direction (Figure 3). Thus, Loewenstein's rule[20] is obeyed in contrast to our previously reported $Sr[B_2O(SO_4)_3]$.[11] Each borate tetrahedron is connected to four adjacent sulfate tetrahedra, whereas the sulfate tetrahedra itself are connected to two adjacent borate tetrahedra. The resulting chain of four membered rings can be described as loop branched *vierer* single chain with the Niggli formula $\{^{1}_{\infty}[B(SO_4)_{4/2}]^{2-}\}$. In contrast to $(NH_4)_3[B(SO_4)_3]$, a lower B:S ration of 1:2 still leads to chains instead of layers or – looking at silicate chemistry – three-dimensional frameworks. This can be explained by the presence of edge sharing supertetrahedra, adopting the chain topology in SiS_2.[21]

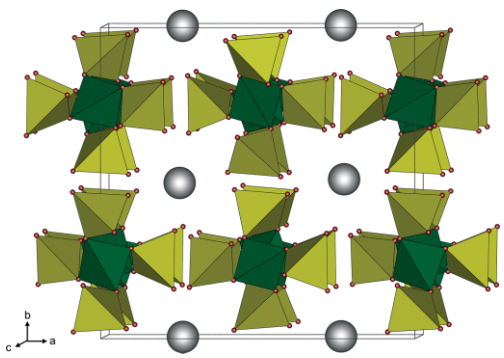

Figure 3. Crystal structure of $Sr[B_2(SO_4)_4]$ viewed along (001); sulfate tetrahedra yellow, borate tetrahedra green, strontium atoms grey.

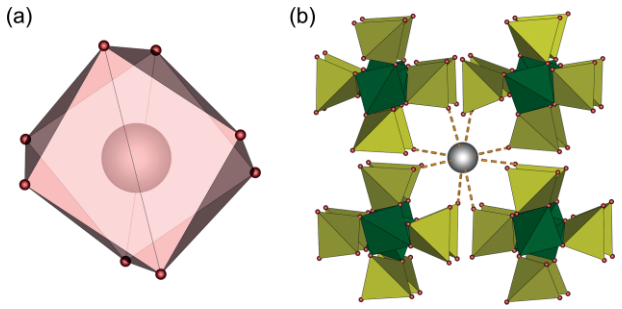

Figure 4. (a) Distorted square antiprismatic coordination of Sr and (b) extended coordination environment.

In the borate tetrahedron the bond lengths B–O are in the range of 146.5(6)–147.1(6) pm (Table 3). Within the sulfate tetrahedra shorter S–O^{br} bonds with values of 141.7(3)–142.3(3) pm and longer S–O^{term} bonds with values between 152.6(3)–154.5(3) pm are observed. All tetrahedra can be classified as regular ones, as the deviation from the tetrahedral symmetry[17,18] for the borate tetrahedron is –0.49 % and for the sulfate tetrahedra between –0.15 and –0.50 %. The higher rigidity within the edge sharing BS_4 supertetrahedron lead to a deviation of –6.38 %, which is larger than for the more flexible corner sharing supertetrahedron in $(NH_4)_3[B(SO_4)_3]$. The charge compensating strontium cations are located on the special Wyckoff position 4*c*. Herein, the single crystallographically independent site is fully occupied, whereas in $Pb[B_2(SO_4)_4]$ the metal cations are disordered, which leads to two crystallographically independent sites (both on 4*c*) with occupation factors of 94.4 and 5.6 %, respectively.[13] They are coordinated by eight oxygen atoms stemming from the four adjacent chains (Figure 4). The Sr–O distances range between 254.0(3) and 270.4(3) pm and are hence within the sum of the ionic radii ($\sum r_{ion}$ = 210 pm).[22]

Finally, the anionic chains in $(NH_4)_3[B(SO_4)_3]$ and $Sr[B_2(SO_4)_4]$ are compared to each other and to their corresponding silicate-analogue structures (Figure 5).

MAPLE

Both crystal structures were checked for their electrostatically consistency by calculations based on the *MAPLE* (*MA*delung *P*art of *L*attice *E*nergy) concept.[23–25] The *MAPLE* values for $(NH_4)_3[B(SO_4)_3]$ and $Sr[B_2(SO_4)_4]$ were calculated and compared to the values of their binary, ternary and quaternary constituents like SO_3,[26] $B_2S_2O_9$,[27] $(NH_4)_2SO_4$[28] and $SrSO_4$,[29] respectively. Both presented structures show a deviation well below 1 % and thus show electrostatic consistency (Table 2).

Table 2. Calculated *MAPLE* values for $(NH_4)_3[B(SO_4)_3]$ and $Sr[B_2(SO_4)_4]$ compared to the sum of the *MAPLE* values for $B_2S_2O_9$, SO_3 and $(NH_4)_2SO_4$ or $SrSO_4$.

$2(NH_4)_3[B(SO_4)_3]$ *MAPLE* = 284320 kJ·mol^{-1} (Δ = 0.4 %)	$3(NH_4)_2SO_4$[28] + $B_2S_2O_9$[27] + SO_3[26] *MAPLE* = 283291 kJ·mol^{-1}
$Sr[B_2(SO_4)_4]$ *MAPLE* = 145390 kJ·mol^{-1} (Δ = 0.4 %)	$SrSO_4$[29] + $B_2S_2O_9$[27] + SO_3[26] *MAPLE* = 144868 kJ·mol^{-1}

Vibrational Spectroscopy

The results of Fourier-transformed infrared (FT-IR) spectroscopy confirm the presence of borate and sulfate tetrahedra

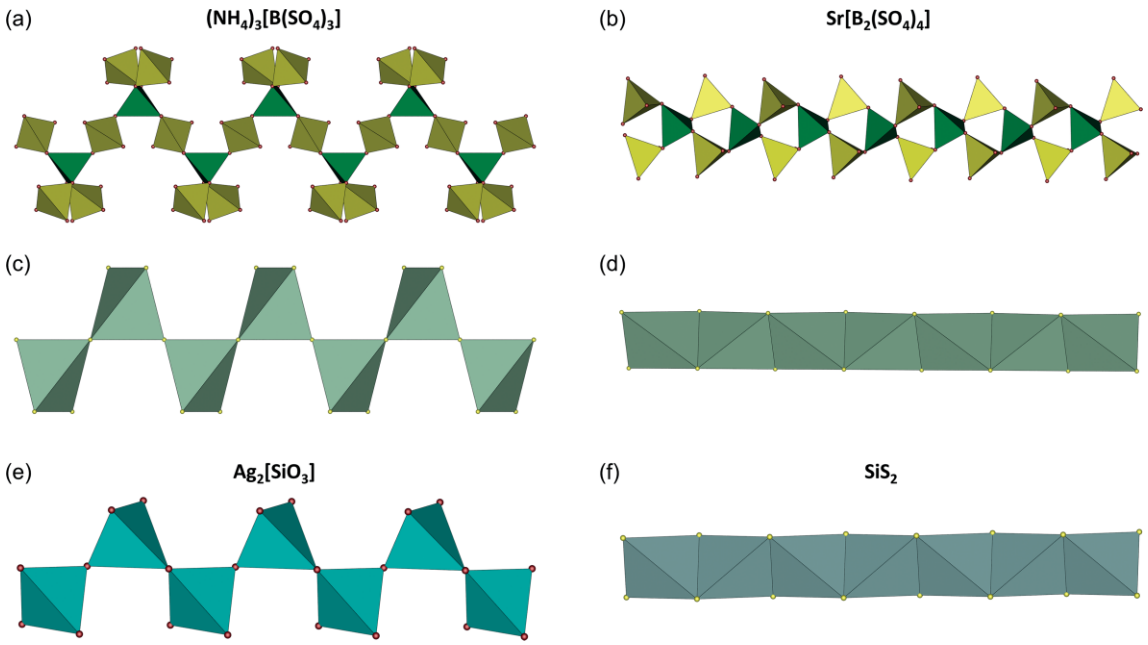

Figure 5. (a) Open branched *vierer* single chain and (c) corner sharing BS_4 supertetrahedra (mint green) in $(NH_4)_3[B(SO_4)_3]$, (b) loop branched *vierer* single chain and (d) edge sharing BS_4 supertetrahedra (mint green) in $Sr[B_2(SO_4)_4]$; (e) unbranched *zweier* single chain (silicate tetrahedra: blue) in $Ag_2[SiO_3]$ and (f) edge sharing SiS_4 tetrahedra (grey) in SiS_2.

in both crystal structures, $(NH_4)_3[B(SO_4)_3]$ and $Sr[B_2(SO_4)_4]$, and are in good agreement with reported data of structurally similar borosulfates.[5,13] The infrared spectrum of $(NH_4)_3[B(SO_4)_3]$ is depicted in Figure 6 and shows striking similarities to $K_3[B(SO_4)_3]$. Furthermore, a tentative assignment based on the calculations on $Ag[B(SO_4)_2]$ is made, as the chains solely contain sulfate and borate tetrahedra.[30]

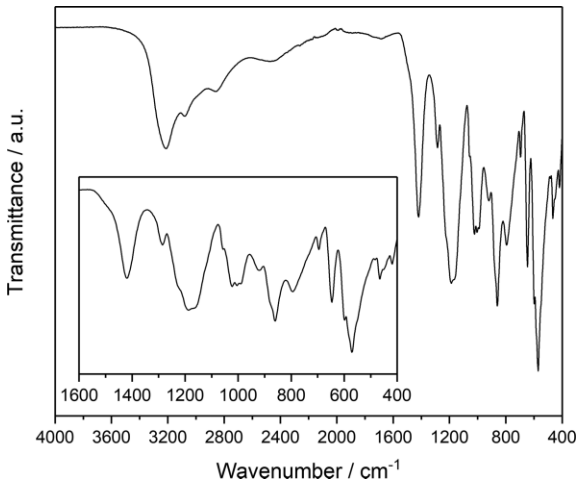

Figure 6. Infrared spectrum of $(NH_4)_3[B(SO_4)_3]$ in the range of 4000 to 400 cm^{-1}, with an inset in the range of 1600 to 400 cm^{-1}.

As reported in literature, the N–H modes of the NH_4^+ cation are found around 3200 cm^{-1}.[7] The asymmetric stretching vibrations ν_{asym}(S–O) can be found in the region 1420–1190 cm^{-1}, while the bands at 1060 and 1020 cm^{-1} can be assigned to the symmetric stretching vibrations ν_{sym}(B–O). Symmetric stretching vibrations ν_{sym}(S–O) and asymmetric bending vibrations δ_{asym}(OSO) are recorded in the region between 920 and 694 cm^{-1}. Below 650 cm^{-1} bending vibrations of the sulfate and borate tetrahedra dominate the spectrum.

In Figure 7 the infrared spectrum of $Sr[B_2(SO_4)_4]$ is shown (full spectrum in Figure S1, Supporting Information). Due to the same anionic chains in $Ag[B(SO_4)_2]$ and $Cu[B_2(SO_4)_4]$, the bands are assigned to calculations therein.[30,31] The region between 1450 and 1100 cm^{-1} can be assigned to asymmetric stretching vibrations ν_{asym}(S–O), with two sharp bands at 1342 cm^{-1} and 1207 cm^{-1}. Symmetric and asymmetric stretching vibrations ν(B–O) can be found at 1078 and 1020 cm^{-1}, respectively. The bands at 985 and 873 cm^{-1} are attributed to bending vibrations δ(OBO), whereas a symmetric bending vibration ν_{asym}(S–O) is visible at 925 cm^{-1}. Asymmetric bending vibrations δ(OBO) and δ(SOB) occur at 663 and 621 cm^{-1}, respectively. Collective bending vibrations δ(OBO/OSO) dominate the spectrum between 542 and 519 cm^{-1} and asymmetric bending vibrations δ(OSO) are assigned to the bands below 500 cm^{-1}.

Thermal Analysis

Thermal analysis on borosulfates sometimes yield further compounds, e.g. in $K_3[B(SO_4)_3]$, a thermal decomposition

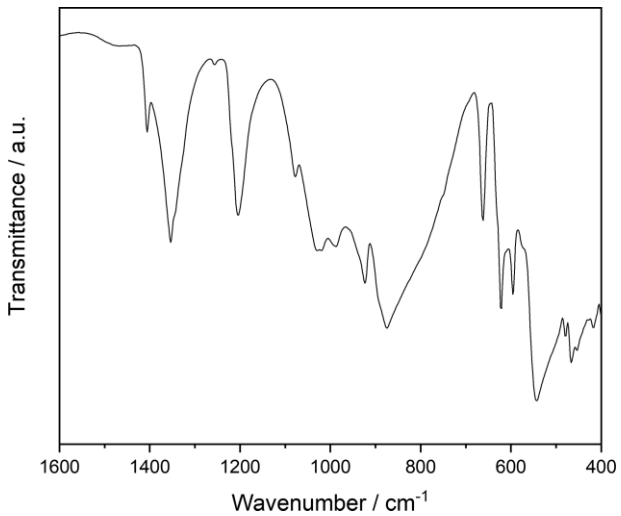

Figure 7. Infrared spectrum of $Sr[B_2(SO_4)_4]$ in the range of 1600 to 400 cm^{-1}.

towards the lower condensed borosulfate $K_5[B(SO_4)_4]$ was reported.[5] Hence, the motivation of the thermal analysis on the structurally similar $(NH_4)_3[B(SO_4)_3]$ was to check, whether a comparable decomposition would yield the hitherto unknown $(NH_4)_5[B(SO_4)_4]$.

As seen in Figure 8, $(NH_4)_3[B(SO_4)_3]$ decomposes in two overlapping steps starting at 320 °C. The total observed mass loss of 87.3 wt% can be explained well by the expulsion of 3 mol SO_3, 3 mol NH_3 and 1.5 mol H_2O per mole $(NH_4)_3[B(SO_4)_3]$ with a calculated mass loss of 90.1 wt%. The slight deviation may be due to residual B_2O_3 caused by a small excess during the synthesis. The larger first step indicates that the release of SO_3 precedes the release of NH_3 and H_2O. The complete decomposition can be assumed according to the following reaction equation:

$$(NH_4)_3[B(SO_4)_3] \rightarrow 0.5\ B_2O_3 + 3\ SO_3\ (g) + 3\ NH_3\ (g) + 1.5\ H_2O\ (g)$$

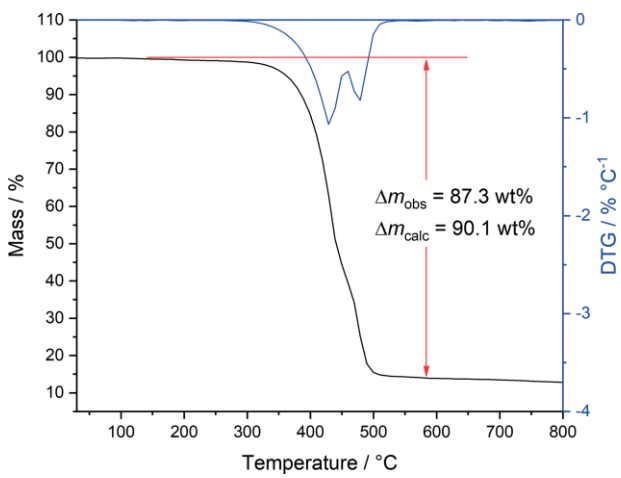

Figure 8. Thermal analysis of $(NH_4)_3[B(SO_4)_3]$ in a nitrogen atmosphere with a heating rate of 10 K·min^{-1}

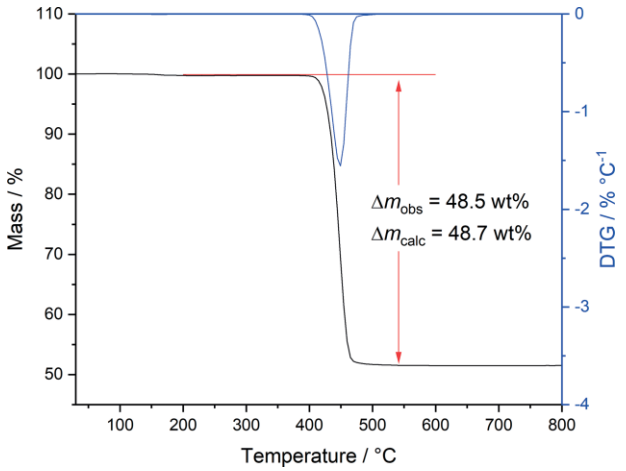

Figure 9. Thermal analysis of $Sr[B_2(SO_4)_4]$ under nitrogen atmosphere with a heating rate of 5 K·min^{-1}.

Furthermore, the thermal behavior of $Sr[B_2(SO_4)_4]$ was investigated (Figure 9). The compound starts to decompose at 400 °C according to the following reaction scheme:

$$Sr[B_2(SO_4)_4] \rightarrow SrSO_4 + B_2O_3 + 3\ SO_3\ (g)$$

The corresponding calculated mass loss of 48.7 wt% due to the evaporation of three moles SO_3 per mole $Sr[B_2(SO_4)_4]$ is in excellent accordance with the observed one of 48.5 wt%. The presence of $SrSO_4$ as only crystalline residue was proven by powder XRD (Figure S2, Supporting Information).

These findings rule out the thermal decomposition of $(NH_4)_3[B(SO_4)_3]$ towards the lower condensed borosulfate $(NH_4)_5[B(SO_4)_4]$, as well as the decomposition of $Sr[B_2(SO_4)_4]$ towards $Sr[B_2O(SO_4)_3]$. However, a thermal treatment of $Sr[B_2(SO_4)_4]$ in the mother liquor at 300 °C, yields a transformation towards $Sr[B_2O(SO_4)_3]$ (Figure S3, Supporting Information). Presumably, the excess of sulfuric acid and oleum embanks the release of SO_3 in a manner, that $Sr[B_2O(SO_4)_3]$ can form.

Conclusions

Herein, we reported the crystal structures of $(NH_4)_3[B(SO_4)_3]$, crystallizing homeotypic to $K_3[B(SO_4)_3]$ as well as $Sr[B_2(SO_4)_4]$, which crystallizes as an ordered variant of $Pb[B_2(SO_4)_4]$. We classify both compounds as conventional borosulfates with anionic chains. However, their connection patterns differ from open branched *vierer* single chains or corner sharing supertetrahedra, respectively, in $(NH_4)_3[B(SO_4)_3]$ to loop branched *vierer* single chains or edge sharing supertetrahedra, respectively, in $Sr[B_2(SO_4)_4]$. This difference originates from the different synthesis approaches and is in accordance with previous results: edge sharing supertetrahedra were up to now solely obtained by solvothermal approaches using oleum, precipitations in oleum or decompositions of borosulfates comprising disulfate groups, e.g. $A[B(S_2O_7)_2]$ (A = NH_4, Na, K). Corner sharing supertetrahedra were achieved by open vessel reactions with sulfuric acid or solid state syntheses using metal disulfates.

Thermal analysis on $(NH_4)_3[B(SO_4)_3]$ showed, that a straight thermal decomposition towards $(NH_4)_5[B(SO_4)_4]$ is not possible, whereas $Sr[B_2(SO_4)_4]$ can only be decomposed towards $Sr[B_2O(SO_4)_3]$ in an excess of the mother liquor present. This is in good agreement with reported results on $Mg[B_2(SO_4)_4]$, where the evaporation of the mother liquor also yielded a borosulfate containing B-O-B-bridges, namely $Mg_4[B_2O(SO_4)_6]$.

To sum up, these findings suggest a possible decomposition of known borosulfates, comprising edge sharing supertetrahedra towards borosulfates containing B–O–B bridges, and point out once more the vast structural diversity of borosulfates – even within a considered cation.

Experimental Section

Synthesis: $(NH_4)_3[B(SO_4)_3]$: 3 mmol (0.3964 g) of $(NH_4)_2SO_4$ and 2.2 mmol (0.1360 g) of $B(OH)_3$ were transferred to a porcelain crucible. 2 mL H_2SO_4 and 0.2 mL oleum (65 % SO_3) were added and the crucible was placed in a muffle furnace inside a fume hood, applying the following heating program: heating to 300 °C within 3 h, holding this temperature for 24 h, followed by rapid cooling. $(NH_4)_3[B(SO_4)_3]$ was obtained quantitatively as phase pure, colorless, slightly moisture sensitive crystals. $Sr[B_2(SO_4)_4]$ was synthesized in analogy to $Ca[B_2(SO_4)_4]$.[10] 0.5 mmol (0.0738 g) of $SrCO_3$, 1.6 mmol (0.0989 g) of $B(OH)_3$, 0.2 mL H_2SO_4 and 0.8 mL oleum (65 % SO_3) were transferred into a silica glass ampule (outer diameter: 1.2 cm, wall thickness: 0.1 cm, length: 15 cm). The fused ampule was transferred to a muffle furnace and the following heating program was applied: heating to 180 °C within 3 h, holding this temperature for 24 h and cooled down to room temperature within 25 h. Colorless single crystals were formed in the acid. The ampules were opened after cooling down with liquid nitrogen. The excess acid was decanted and the crystals were washed with dry acetonitrile and vacuum filtered. The yield was almost quantitative and the moisture sensitive crystals were transferred into an argon glove box. The phase-purity of $(NH_4)_3[B(SO_4)_3]$ and $Sr[B_2(SO_4)_4]$ was confirmed by Rietveld refinements (Figure 10).

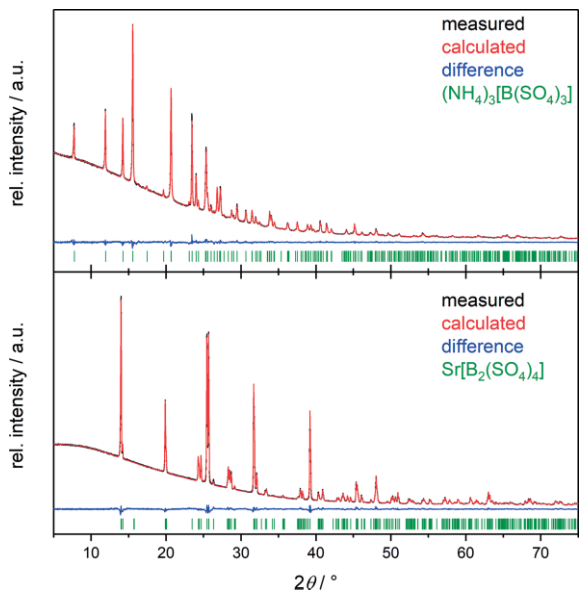

Figure 10. Rietveld refinement of $(NH_4)_3[B(SO_4)_3]$ (top) and $Sr[B_2(SO_4)_4]$ (bottom); measured (black line) and calculated (red line) powder diffraction pattern; theoretical reflection positions (green vertical bars) and the difference plot (blue line).

Crystal Structure Determination: Single-crystals were transferred into perfluorated polyether and selected for single-crystal XRD. Diffraction data for all compounds were collected with a Bruker D8 Venture diffractometer using Mo-K_α radiation (λ = 0.71073 Å). The temperature was adjusted with a nitrogen flow (Oxford Cryosystems). The absorption correction was performed employing the multi-scan method;[32] then the crystal structures were solved with direct methods within the SHELXS program[33] and refined by the full-matrix least-squares technique within the SHELXTL program.[34] The position of the hydrogen atoms in $(NH_4)_3[B(SO_4)_3]$ was located by peaks in the difference Fourier map and fixed to nitrogen with a bond length of 99(1) pm. $Sr[B_2(SO_4)_4]$ was refined as pseudo merohedral twin applying the twin law (0 1 0 1 0 0 0 0 –1). Further details of the crystal structure investigations discussed in this contribution are listed in Table 3 as well as in Tables S1–S4 (Supporting Information).

Table 3. Crystal data and details of the structure refinements of $(NH_4)_3[B(SO_4)_3]$ and $Sr[B_2(SO_4)_4]$ (esds in parantheses).

	$(NH_4)_3[B(SO_4)_3]$	$Sr[B_2(SO_4)_4]$
Temperature /K	200(2)	250(2)
Molar weight /g·mol^{-1}	353.12	493.48
Crystal system	orthorhombic	orthorhombic
Space group	*Ibca* (no. 73)	*Pnna* (no. 52)
a /pm	728.58(3)	1257.4(4)
b /pm	1470.84(7)	1242.1(4)
c /pm	2270.52(11)	731.9(2)
Volume /10^6 pm^3	2433.15(19)	1143.1(6)
Z	8	4
Calculated density D_x/ g·cm^{-3}	1.928	2.867
Absorption coefficient μ / mm^{-1}	0.677	5.550
F(000)	1456	960
Diffractometer	Bruker D8 Venture	Bruker D8 Venture
Radiation (λ /Å)	0.71073	0.71073
Absorption correction	multi-scan	multi-scan
Theta range /°	2.770 < θ < 33.045	2.305 < θ < 26.466
Index range *h*|*k*|*l* (min./ max.)	–11/10|–13/22|–32/ 34	–15/15|–15/15|–6/ 9
Reflections collected	13656	10124
Independent reflections	2314	1221
Observed reflections ($I >$ 2σ)	1964	919
Refined parameters/ restraints	106 / 6	107 / 0
R_{int}	0.0383	0.0824
R_1 (all data)	0.0426	0.0569
wR_2 (all data)	0.0908	0.0705
GooF	1.087	1.013
Residual electron density min./max. /e–·Å^{-3}	–0.502/0.626	–0.626/0.572

Further details of the crystal structures investigations may be obtained from the Fachinformationszentrum Karlsruhe, 76344 Eggenstein-Leopoldshafen, Germany (Fax: +49-7247-808-666; E-Mail: crysdata@fiz-karlsruhe.de, http://www.fiz-karlsruhe.de/request for deposited data.html) on quoting the depository numbers CSD-1987105 for $Sr[B_2(SO_4)_4]$ and CSD-1987106 for $(NH_4)_3[B(SO_4)_3]$.

X-ray Powder Diffraction: The samples were ground and filled into a Hilgenberg glass capillary (outer diameter 0.3 mm, wall thickness 0.01 mm) inside a glovebox. The data was collected with a Bruker D8 Advance diffractometer with Cu-K_α radiation (λ = 154.184 pm) with a 1D LynxEye detector. Rietveld refinement was done using the program TOPAS V.[35] Details on the Rietveld refinement are displayed in Table S5 (Supporting Information).

Infrared Spectroscopy: The infrared spectra were recorded using a Bruker EQUINOX 55 FT-IR spectrometer equipped with a platinum ATR setup in a range of 4000–400 cm^{-1}.

Thermal Analysis: The thermogravimetric analysis was done in alumina crucibles employing a NETZSCH STA 409 PC Luxx in a nitrogen atmosphere and a heating ramp of 10 K·min^{-1} and 5 K·min^{-1}, respectively.

Supporting Information (see footnote on the first page of this article): The supporting information contains crystallographic tables of both compounds, details on the Rietveld refinement, the full IR spectrum of $Sr[B_2(SO_4)_4]$ and powder XRD pattern of the decomposed samples of $Sr[B_2(SO_4)_4]$.

Acknowledgements

The authors thank the Deutsche Forschungsgemeinschaft (DFG) for financial support under the project HO 4503/5–1. P.N. thanks the Fonds der Chemischen Industrie (FCI) for a Ph.D. fellowship. Open access funding enabled and organized by Projekt DEAL.

Keywords: Borosulfates; Structure elucidation; Ammonium; Strontium; Thermal analysis

References

[1] F. Liebau, *Structural Chemistry of Silicates*, Springer, Heidelberg, **1985**.
[2] J. Bruns, H. A. Höppe, H. Hillebrecht, M. Daub, H. Huppertz, *Chem. Eur. J.* **2020**, doi: 10.1002/chem.201905449.
[3] F. Stadler, O. Oeckler, J. Senker, H. A. Höppe, P. Kroll, W. Schnick, *Angew. Chem. Int. Ed.* **2005**, *44*, 573.
[4] H. A. Höppe, K. Kazmierczak, M. Daub, K. Förg, F. Fuchs, H. Hillebrecht, *Angew. Chem. Int. Ed.* **2012**, *51*, 6255.
[5] M. Daub, K. Kazmierczak, P. Gross, H. Höppe, H. Hillebrecht, *Inorg. Chem.* **2013**, *52*, 6011.
[6] M. Daub, H. Hillebrecht, *Eur. J. Inorg. Chem.* **2015**, *2015*, 4176.
[7] M. Daub, H. A. Höppe, H. Hillebrecht, *Z. Anorg. Allg. Chem.* **2014**, *640*, 2914.
[8] M. Daub, K. Kazmierczak, H. A. Höppe, H. Hillebrecht, *Chem. Eur. J.* **2013**, *19*, 16954.
[9] P. Netzsch, P. Gross, H. Takahashi, H. A. Höppe, *Inorg. Chem.* **2018**, *57*, 8530.
[10] J. Bruns, M. Podewitz, M. Schauperl, B. Joachim, K. R. Liedl, H. Huppertz, *Chem. Eur. J.* **2017**, *23*, 16773.
[11] P. Netzsch, P. Gross, H. Takahashi, S. Lotfi, J. Brgoch, H. A. Höppe, *Eur. J. Inorg. Chem.* **2019**, *2019*, 3975.
[12] P. Gross, A. Kirchhain, H. A. Höppe, *Angew. Chem. Int. Ed.* **2016**, *55*, 4353.
[13] S. Schönegger, J. Bruns, B. Gartner, K. Wurst, H. Huppertz, *Z. Anorg. Allg. Chem.* **2018**, *644*, 1702.
[14] R. Kniep, G. Gözel, B. Eisenmann, C. Röhr, M. Asbrand, M. Kizilyalli, *Angew. Chem. Int. Ed. Engl.* **1994**, *33*, 749.
[15] M. Jansen, K. Heidebrecht, R. Matthes, W. Eysel, *Z. Anorg. Allg. Chem.* **1991**, *601*, 5.
[16] P. Netzsch, M. Hämmer, P. Gross, H. Bariss, T. Block, L. Heletta, R. Pöttgen, J. Bruns, H. Huppertz, H. A. Höppe, *Dalton Trans.* **2019**, *48*, 4387.
[17] E. Makovicky, T. Balić-Žunić, *Acta Crystallogr., Sect. B* **1998**, *54*, 766.

[18] T. Balić Žunić, E. Makovicky, *Acta Crystallogr., Sect. B* **1996**, *52*, 78.
[19] T. Steiner, *Angew. Chem. Int. Ed.* **2002**, *41*, 48.
[20] W. Loewenstein, *Am. Mineral.* **1954**, *39*, 92.
[21] J. Peters, B. Krebs, *Acta Crystallogr., Sect. B* **1982**, *38*, 1270.
[22] R. D. Shannon, *Acta Crystallogr., Sect. A* **1976**, *32*, 751.
[23] R. Hoppe, *Angew. Chem.* **1966**, *78*, 52.
[24] R. Hoppe, *Angew. Chem. Int. Ed. Engl.* **1970**, *9*, 25.
[25] R. Hübenthal, MAPLE. Program for the Calculation of the Madelung Part of Lattice Energy, Universität Gießen, **1993**.
[26] R. Pascard, C. Pascard-Billy, *Acta Crystallogr.* **1965**, *18*, 830.
[27] C. Logemann, M. S. Wickleder, *Angew. Chem. Int. Ed.* **2013**, *52*, 14229.
[28] E. O. Schlemper, W. C. Hamilton, *J. Chem. Phys.* **1966**, *44*, 4498.
[29] D. Garske, D. R. Peacor, *Z. Kristallogr.* **1965**, *121*, 204.
[30] J. Bruns, M. Podewitz, M. Schauperl, K. R. Liedl, O. Janka, R. Pöttgen, H. Huppertz, *Eur. J. Inorg. Chem.* **2017**, 3981.
[31] J. Bruns, M. Podewitz, K. R. Liedl, O. Janka, R. Pöttgen, H. Huppertz, *Angew. Chem. Int. Ed.* **2018**, *57*, 9548.
[32] Bruker, *SADABS*, Bruker AXS Inc., Madison, Wisconsin, USA, **2001**.
[33] G. M. Sheldrick, *Acta Crystallogr., Sect. A* **2008**, *64*, 112.
[34] G. M. Sheldrick, *Acta Crystallogr., Sect. C* **2015**, *71*, 3.
[35] Bruker, Topas V5. General profile and structure analysis software for powder diffraction data, Karlsruhe, Germany, **2014**.

Received: February 28, 2020
Published Online: May 5, 2020

